ELSEVIER

Chemical Engineering Science 62 (2007) 4479–4495

Chemical Engineering Science

www.elsevier.com/locate/ces

Numerical predictions of flow patterns due to natural convection in a vertical slot

A.A. Ganguli, A.B. Pandit*, J.B. Joshi

Institute of Chemical Technology, University of Mumbai, Matunga, Mumbai 400019, India

Received 10 November 2006; received in revised form 30 April 2007; accepted 4 May 2007
Available online 23 May 2007

Abstract

Natural convection in rectangular slots has vital applications in cooling of nuclear reactor insulation, chemical vapor deposition, insulation of double pane windows, environmental processes, and phase change processes. Flow patterns arising out of density differences depend on height to width ratio (aspect ratio (AR)) and temperature difference. These flow patterns have a significant effect on rate of heat transfer. Hence flow patterns in a slender vertical slot with large height to width ratio (AR = 20) have been numerically studied for four fluids (mercury, air, and water and silicon oil) of varying Prandtl numbers. The circulation cell formation and merging has been seen as a quasi-periodic behavior for water and silicon oil at various Rayleigh numbers. The genesis of formation of circulation cells due to the pressure differentials (as a result of thermal gradients) has been satisfactorily explained for mercury, air, and water and silicon oil and a criterion for the same has been developed for the range of Prandtl number between 0.71 and 7 on the basis of numerical predictions.

Keywords: Computational fluid dynamics; Rectangular slots; Flow patterns; Multicellular convection; Natural convection; Heat transfer

1. Introduction

Natural convection in enclosures in rectangular slots with differentially heated end walls has been studied experimentally as well as analytically extensively over the years (Batchelor, 1954; Elder, 1965; Gill, 1966; Rubel and Landis, 1969; Newell and Schmidt, 1970; Quon, 1972; Bergholz, 1978; Catton, 1978; Lee and Korpela, 1983; Le Quéré, 1990; Wakitani, 1996; Lartigue et al., 2000; Chan et al., 2004). Heat transfer in buoyancy-dominated flows is of fundamental importance in several engineering applications. Relevant examples include nuclear reactor insulation, chemical vapor deposition (CVD), applications in chemical, food and metallurgical industries, environmental processes, cooling of electronic equipment, crystal growth, phase-change processes and passive solar heating. The flow patterns in all these cases are extremely sensitive to the changes in cavity configuration and the imposed boundary conditions (adiabatic conditions or free surfaces at the top and the bottom, heating and cooling temperatures at the sides). Fig. 1 shows a typical vertical slot with height H and width L. Constant temperature is maintained at the left and right walls such that left wall is heated and right wall is cooled while the top and the bottom are insulated. Due to the temperature gradient arising between the left and right walls, fluid rises along the hot wall, turns in the top end, sinks along the cold wall, and turns again around at the bottom to set up unicellular convection. Three dimensionless parameters describe the flow namely the Rayleigh number (Ra) (ratio of buoyancy to viscous forces) ($g\beta\Delta TL^3/\nu\alpha$), the Prandtl number, $Pr(C_p\mu/k)$ (ratio of momentum to thermal diffusivity) and the aspect ratio, AR (H/L) (height to width ratio). The flows are classified into three regimes: the conduction regime, the transitional regime and the boundary layer regime. In the conduction regime, the temperature varies linearly across the cavity; hence the heat transfer rate between the two side walls is of the order $kH\Delta T/L$. The horizontal temperature gradient $\Delta T/L$ gives rise to a slow, clockwise circulation, however, the heat transfer contribution of this flow is insignificant. In the boundary layer regime, vertical thermal boundary layers form distinctly along the differentially heated sidewalls. The heat transfer rate across the cavity scales as $(k/\delta_T)H\Delta T$. The adiabatic horizontal walls are lined by distinct thermal layers.

* Corresponding author. Tel.: +91 22 2414 5616; fax: +91 22 2414 5614.
E-mail address: abp@udct.org (A.B. Pandit).

0009-2509/$ - see front matter © 2007 Elsevier Ltd. All rights reserved.
doi:10.1016/j.ces.2007.05.017

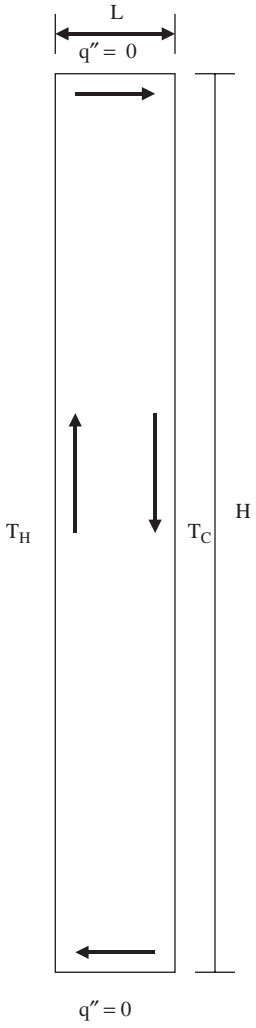

Fig. 1. Schematic of a rectangular slot differentially heated and cooled from both sides.

Most of the cavity core is relatively stagnant and has uniform temperature. However, in the transition regime the boundary layers at the hot and cold walls meet each other. To summarize, conduction regime is governed by conduction, transition regime by conduction near the walls and convection in the core and boundary layer regime by convection in the core and conduction limited to the boundary layer. In the convection dominated region (the core) multiple cells are formed. At low *Ra* values ($3000 < Ra < 10^4$, depending on the values of AR, $5 < \mathrm{AR} < 40$ and $0.01 < Pr < 224$) the cells form and remain steady for infinite time. These have been termed as secondary cells (Elder, 1965). For higher *Ra* ($10^4 < Ra < 10^6$ depending on the values of AR, $5 < \mathrm{AR} < 110$ and $0.01 < Pr < 224$) the cells move and merge. These cells form between secondary cells and take the form of cells rotating in clockwise direction and assist in the cell merging process. These are termed as tertiary cells (Elder, 1965).

1.1. Previous work

The quest to understand the effect of the three dimensionless parameters (*Ra*, *Pr* and AR) on the heat transfer rates due to natural convection in rectangular slots has been going on since 1930. These efforts can be classified as analytical approach (Batchelor, 1954; Elder, 1965; Gill, 1966; Korpela et al., 1973), experimental studies (Mull and Reiher, 1930; Elder, 1965; Yin et al., 1978; Elsherbiny et al., 1982; Wakitani, 1996; Chan et al., 2004) and numerical studies (Newell and Schmidt, 1970; Korpela et al., 1982; Lee and Korpela, 1983; Le Quéré, 1990; Wakitani, 1994, 1997; Zhao et al., 1997; Lartigue et al., 2000; Chan et al., 2004). Table 1

A–C summarizes the numerical and experimental details, the assumptions made by the different researchers and the conclusions drawn from the analysis by various authors. Batchelor (1954) investigated the heat transfer due to free convection in high AR slots ($\mathrm{AR} \geqslant 10$). He analytically solved velocity distribution for a rectangular slot. Analogy with the formation of thermal boundary layer on a vertical flat plate was considered and from the velocity distribution a criterion for critical Rayleigh number (Ra_c) was predicted at which the flow instability occurs. In the range $10^5 < Ra < 10^7$ he found that heat transfer was significantly enhanced by convective cells and the conduction dominated region was restricted in thin layer at the wall. He analyzed the different flow regimes (conduction and boundary layer regime) at different *Ra* number and AR and found a criterion for the flow to be laminar or turbulent. Elder (1965) investigated the natural convection of a viscous fluid (silicon oil and paraffin oil) in a vertical slot with an objective to understand the interaction between buoyancy and shearing forces. He further carried out flow visualization studies to understand the mechanism of onset of convective cells. He, performed experiments over a wide range of *Ra* number with a high *Pr* number fluid (silicon oil, $Pr = 224$) and predicted flow patterns over the range considered (Table 1B). He concluded that for $Ra < 1000$the flow remained unicellular and stable. In the range $1000 < Ra < 10^5$ the flow was similar to that of flow on vertical plates with boundary layer being formed at the two vertical walls and uniform velocity gradient in the core region. Near $Ra = 10^5$ a steady secondary flow pattern, i.e., 'cat's eye' (Fig. 2) pattern was seen which is superimposed on the mean flow. Above $Ra = 10^7$ he observed the onset of turbulence. Gill (1966) considered the case of high temperature difference ($\Delta T > 50$, $Ra > 10^5$) in which transfer of heat from one vertical wall to other was mainly by convection and heat transfer by conduction was only in the thin boundary layers adjoining the walls. He validated the results of experiments conducted by Elder (1965) with his approximate analytical approach and found that his results were agreeable with practically all the experimental results of Elder (1965). Some differences with experimental results were found with predictions of Gill (1966) which was attributed to the variation in viscosity with temperature which occurred in the experiments. Newell and Schmidt (1970) solved steady state governing equations of mass, momentum and energy over a wide range of Grashoff numbers ($g\beta\Delta T\rho^2 L^3/\mu^2$) ($4 \times 10^3 \leqslant Gr \leqslant 1.4 \times 10^6$) ($2 < \mathrm{AR} < 20$) with air as a working fluid ($Pr = 0.73$) with an objective to obtain relationship between the convective heat transfer coefficient and the imposed boundary conditions. On the basis of the numerical results they first proposed

Table 1
(A) Details of various geometry, range and proposed correlations available in literature; (B) Details of experimental techniques used by different researchers; (C) Solution schemes used by earlier researchers

Author	Fluid	Geometry details (aspect ratio range)	Range of Rayleigh/Grashoff number	Proposed correlations and Nusselt numbers
(A)				
Batchelor (1954)	Air	–	$10^3 < Ra < 10^7$	–
Elder (1965)	Paraffin, silicon oil	$1 < \mathrm{AR} < 60$	$10^3 < Ra < 10^5$	$Ra_c >= 1700\mathrm{AR}$
			$Ra < 10^3$	$Nu = 0.46\left(\frac{Ra}{Pr}\mathrm{AR}^3\right)$
			$Ra < 10^8$	
Gill (1966)	Paraffin, silicon oil	$\mathrm{AR} > 1$	$10^3 < Ra < 10^7$	–
Newell and Schmidt (1972)	Water, air, and $Pr = 900$	$\mathrm{AR} = 1$	$4 \times 10^3 < Gr < 1.4 \times 10^6$	$Nu = 0.0547(Gr)^{0.3947}$
		$\mathrm{AR} = 5$	10^6	$Nu = 0.155(Gr)^{0.315}\ (\mathrm{AR})^{-0.265}$
Yin et al. (1978)	Air	4.9 $< \mathrm{AR} < 78.7$	$1500 < Ra < 7 \times 10^6$	$0.21Gr^{0.269}\mathrm{AR}^{-0.131}$
Elsherbiny et al. (1982)	Air	$5 < \mathrm{AR} < 110$	$1000 < Ra < 10^7$	$Nu_1 = 0.0605Ra^{1/3}$ $Nu_2 = [1 + \{0.104Ra^{0.293}/1 + (6310/Ra)^{1.36}\}^3]^{1/3}$ $Nu_3 = 0.242(Ra/A)^{0.272}$ $Nu = [Nu_1, Nu_2, Nu_3]_{\max}$
Le Quéré (1990)	Air	$\mathrm{AR} = 16$	$6 \times 10^3 < Ra < 4 \times 10^4$	Table 1Ab
Wakitani (1997)	Air, glycerine	$\mathrm{AR} = 16$	$9 \times 10^3 < Ra < 3 \times 10^5$	–
Zhao et al. (1997)	Air	$10 < \mathrm{AR} < 100$	$3550 < Ra < 5 \times 10^6$	Table 1Ac
Lartigue et al. (2000)	Air	$\mathrm{AR} = 40$	$3550 < Ra < 2 \times 10^4$	Table 1Ad
Chan et al. (2004)	Air	$\mathrm{AR} = 15$ $225 \times 15 \times 75$	Ethanol–water system.	–

(Aa) Lee and Korpela (1983)

AR = 5		AR = 10		AR = 15		AR = 20		AR = 40		AR = 60	
Ra	*Nu*	*Ra*	*Nu*	*Ra*	*Nu*	*Ra*	*Nu*	*Ra*	*Nu*	*Ra*	*Nu*
9.23E + 02	1.0379	2.19E + 03	2.22E + 03	1.0709	1.0954	2.26E + 03	1.044	3.60E + 03	1.0428	2.19E + 03	9.93E − 01
3.57E + 03	1.4352	3.55E + 03	3.66E + 03	1.1443	1.2029	3.59E + 03	1.0978	7.12E + 03	1.1235	3.57E + 03	9.94E − 01
7.11E + 03	1.7873	5.74E + 03	5.67E + 03	1.2579	1.3594	5.03E + 03	1.1528	8.56E + 03	1.2005	4.97E + 03	9.94E − 01
1.06E + 04	2.0367	7.13E + 03	7.21E + 03	1.335	1.4548	5.78E + 03	1.1846	1.07E + 04	1.2787	7.10E + 03	9.93E − 01
		8.60E + 03	8.65E + 03	1.412	1.5403	7.15E + 03	1.2408	1.43E + 04	1.3741	7.95E + 03	1.0611
		1.07E + 04	1.07E + 04	1.5147	1.6626	7.90E + 03	1.2787	1.78E + 04	1.4584	8.60E + 03	1.0929
		1.24E + 04	1.43E + 04	1.6418	1.7384	8.55E + 03	1.3154			9.35E + 03	1.1161
		1.43E + 04	1.78E + 04	1.7506	1.8117	9.40E + 03	1.3496			1.08E + 04	1.1516
		1.61E + 04			1.8802	1.07E + 04	1.4046			1.25E + 04	1.1932
		1.77E + 04			1.9352	1.25E + 04	1.467			1.43E + 04	1.2359
						1.43E + 04	1.5208			1.61E + 04	1.2738
						1.60E + 04	1.5733			1.78E + 04	1.3068
						1.78E + 04	1.6198				

(Ab) Le Quéré (1990) AR = 16

$Ra \times 10^{-3}$	*Nu*
1.6	1.2
2.4	2
2.75	2.2
3.2	2.25
4	2.3

(Ac) Zhao et al. (1997) AR = 40

$Ra \times 10^{-3}$	*Nu*
3.55E + 03	1.063
6.80E + 03	1.158
1.01E + 04	1.277
1.42E + 04	1.399
1.78E + 04	1.487

(Ad) Lartigue et al. (2000) AR = 40

$Ra \times 10^{-3}$	*Nu*
3.55E + 03	1.06E + 00
6.80E + 03	1.17E + 00
1.01E + 04	1.29E + 00
1.42E + 04	1.39E + 00
1.78E + 04	1.48E + 00

Table 1 (*continued*)

Author	Experimental technique			
	Measurement	Equipment for measurement	Accuracy	Range of Ra, Gr and AR
(B)				
Elder (1965)	Visual observation of aluminium suspended in fluid	Aluminium as tracer	The temperature difference ΔT was maintained constant at a difference of 0.05 °C. Velocities are accurate to a difference of 5%. Temperatures are accurate upto 0.01 °C	$1 < \mathrm{AR} < 60$ $10^3 < Ra < 10^5$ $Ra < 10^3$ $Ra < 10^8$ $224 < Pr < 1000$
Yin et al. (1978)	Measurement of heat flux	Thermocouples	Accurate temperature measurements with 20 strip electrical heaters. Mica sheet with Nichrome ribbon wound around. Aluminium plate was used for hot plate while copper was used for cold plates	$1500 < Ra < 7 \times 10^6$ $1000 < Ra < 10^7$ $Pr = 0.73$
Elsherbiny et al. (1982)	Heat flux measurement to measure heat transfer coefficient	Thermocouples	Error in the heat flux was 075 $\mathrm{W/m^2}$. Error in temperature linearity was maintained within 1% at the highest Ra number possible. For high AR the width L was maintained within an uncertainty of 0.1% with high precision machining. Temperature variations within each plate was within 0.02 K	$5 < \mathrm{AR} < 110$ $1000 < Ra < 10^7$ $Pr = 0.73$
Wakitani (1996)	Flow visualization	Aluminium oxide powder as tracer	Temperature measurements were at an accuracy of 0.1 °K. Uncertainty with properties of silicon was less than 1%	$10 < \mathrm{AR} < 20$ $3 \times 10^5 < Ra < 1 \times 10^6$ $125 < Pr < 900$
Chan et al. (2004)	Flow visualization and LAB view	Polycrystalline crystals as tracer	Temperature difference across the tank near the top is approximately 3–5% higher or lower than that at the mid tank, depending on the values of temperature difference	$\mathrm{AR} = 15$

Author		Numerical technique				Assumptions	Conclusion
	Governing equations	Numerical method	Grid	Scheme	Time-step		
(C)							
Batchelor (1954)	Navier Stokes equations	Analytical solutions	–	–	–	1,2,5,8,9,10	1,7
Elder (1965)	Navier Stokes equations	Analytical solutions	–	–	–	1,2,5,8,9, 10	1,2,3
Gill (1966)	Boundary layer equations	Analytical solutions	–	–	–	1,2,3,4,5,7,8,9,10	1
Newell and Schmidt (1972)	Stream-function vorticity	Crank–Nicholson method	40×40	Central difference scheme	0.0001	1,2,3,4,5,6,7,8,9,10	4,5,6
Lee and Korpela (1983)	Navier Stokes equations	FEM, FDM, Galerkin method	17×129	Arakawa scheme	1×10^{-3} $Ra = 2000$; 2×10^{-4} $Ra = 10^5$	1,2,3,4,5,6,7,8,9,10	6,7,10,11
Le Quéré (1990)	Navier Stokes equations	Chebyshev polynomials	–	Third order schemes	0.001	1,2,3,4,5,6,7,8,9,10	8,11,12
Wakitani (1997)	Dimensionless Navier Stokes equations	Euler implicit Adam–Brashforth	Non-uniform grid. 25×121	Third order upwinding	0.0005	1,2,3,4,5,6,7,8,9,10	14

Table 1 (*continued*)

Author	Numerical technique					Assumptions	Conclusion
	Governing equations	Numerical method	Grid	Scheme	Time-step		
Zhao et al. (1997)	Dimensionless Navier Stokes equations	FEM	Non-uniform grid	Upwind scheme	0.0001	1,2,3,4,5,6,7,8,9,10	15
Lartigue et al. (2000)	Dimensionless Navier Stokes equations	FVM	Non-uniform grid	Upwind scheme			16
Chan et al. (2004)	Stream-function vorticity	Arakawa scheme	FEM method	Arakawa scheme	0.0005	1,2,3,4,5,6,7,8,9,10	17

Assumptions and conclusions with numbers specified.

Assumptions: (1) A different condition on the temperature field at the two horizontal boundaries would only alter the solution significantly in the vicinity of these boundaries. (2) Boussinesq approximation is made i.e., density differences are only important in producing buoyancy. (3) Properties of the fluid except viscosity do not change significantly in temperature range $T_h < T_m < T_c$. (4) Variation in viscosity is assumed. (5) Heat transfer by radiation is not included. (6) Length of enclosure is sufficiently large for two-dimensional motion to be assumed. (7) Constant properties except in formulation of buoyancy term. (8) Fluid is Newtonian and incompressible. (9) Flow is laminar and two-dimensional. (10) Appropriateness of fairly general but still idealized thermal boundary conditions.

Conclusions: (1) Flow in a vertical slot (AR > 5) remains laminar till a critical Grashoff number above which it is restricted to the boundary layer. (2) Above $Ra > 1 \times 10^5$ secondary flows (multiple cells) are seen and above $Ra > 1 \times 10^7$ tertiary cells are seen (counter-rotating, moving cells). (3) The possibility that tertiary flows arise from instability of secondary flow. (4) Fine grid gives better predictions of flow patterns. (5) Finite Difference method serves as an important tool for predicting flow patterns for complex geometries with required accuracy. (6) For low Prandtl numbers cells settle down rapidly and no quasiperiodic behavior is obtained. (7) High heat transfer near the bottom of the hot wall and near the top of the cold wall can cause local non-uniformities in wall temperature in these regions. These may be the reason for discrepancy between experiments and theory. (8) Cells increase due to instability with time and after a specific time period reverts back to unicellular pattern. Return to unicellular structure is complex than previously analyzed. (9) Number of cells increase step by step and each change is characterized by hysteresis. (10) Initial condition is very important in the case of numerical simulations. (11) Accurate predictions can be made when numerical simulations are done by gradually increasing the Rayleigh number with second set of simulations taking the initial input from results of first set of simulations. (12) With increase in Rayleigh number different number of cells are formed which may revert back to a steady state or remain quasi-periodic (tertiary waves). (13) When Rayleigh number increases there is onset of tertiary cells formation depending on Pr. (14) Experimental observations show cell merging and moving. (15) There exists a particular set of aspect ratios and Rayleigh numbers in laminar regime in which multiple cells are formed called the multicellular regime. (16) Use of sophisticated instruments (PIV) for carrying out experiments serve as a tool for validating the flow patterns obtained by the numerical results and provides a better insight into the physics of the flow. (17) Pressure work acts as the prime component in formation and merging of cells.

correlations for the estimation of Nusselt number *Nu*, as a function of *Gr* number and AR (Table 1A). The complexity of the flow in the core region and covering a wide range of AR prompted researchers (Yin et al., 1978; Lee and Korpela, 1983) to investigate *Nu* number predictions with better experimental and numericaltechniques especially with air as a working fluid. Yin et al. (1978) carried out investigations on tall cavities to examine the role that AR plays on the temperature field and the heat transfer rate in rectangular enclosures by covering a wide range of AR ($4.9 < \mathrm{AR} < 78.7$). They found that *Nu* number was directly proportional to *Gr* number but inversely proportional to AR though the dependence on AR was weak (Table 1A). Lee and Korpela (1983) analyzed the critical values of *Ra* number Ra_c for the onset of multicellular convection and heat transfer just after its formation. They carried out numerical computations over a wide range of the three dimensionless parameters under consideration (Table 1A) (four fluids of different *Pr* number in the range of 0.001–1000 and various ARs in the range of 10–40). They specified a critical Grashoff number (Gr_c) for the onset of instability over the range of *Pr* number and AR covered in the work. They also observed that when water was used as the working fluid ($\mathrm{AR} = 25$, $Ra = 40,000$, $Pr = 7$), number of cells varied with time and after a certain time period a unicellular pattern existed. Le Quéré (1990) carried out numerical integration of time dependent two-dimensional unsteady governing equations with Boussinesq approximation to provide some additional flow features in a vertical cavity of $\mathrm{AR} = 16$ with air as a working fluid. He confirmed that the instability reverts from multicellular to monocellular with increasing value of *Ra* number. Many researchers (Wakitani, 1996; Zhao et al., 1997; Lartigue et al., 2000; Chan et al., 2004) since then have analyzed the phenomena of unsteadiness (changing number of circulation cells as a function of time) at high *Ra* number with mainly air as a working fluid. Further, Wakitani (1996) carried out both experimental and numerical investigations and studied the effect of variable viscosity on the unsteady nature of multiple cells. He carried out impulsive runs (applying temperature gradient to the slot at time equal to 0 s) and found that transient run matched with his experimental results, i.e., vertical velocity fluctuations at the center were similar for experimental and numerical investigations. The authors, however, observed that the transition of multiple cells did not have any significant effect on the average Nusselt number whether the runs were carried out gradually or impulsively. A significant contribution was made by Zhao et al. (1997) who numerically investigated the multicellular convection in tallcavities ($10 < \mathrm{AR} < 110$) to be able to use it as a tool to more accurately predict heat transfer. They predicted the existence of multicellular regime for air which lies in the laminar range. They also estimated the critical Rayleigh number Ra_c at which the flow instability starts for $\mathrm{AR} = 50$. This "prompted researchers to focus on large AR cavities and direct" their efforts to understand

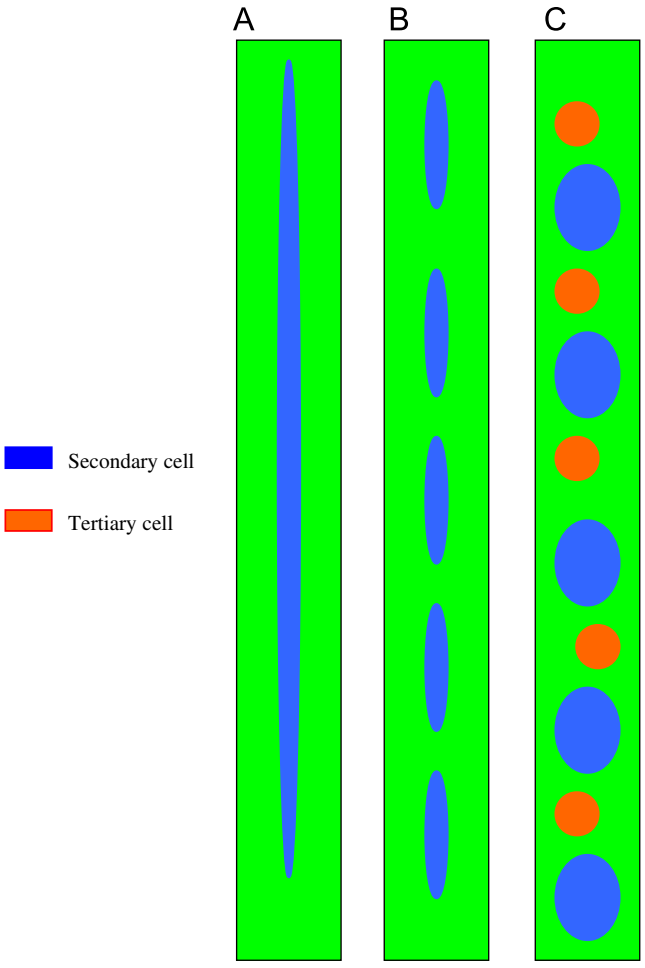

Fig. 2. Schematic of different cellular structures: (A) primary cell; (B) secondary cell; (C) tertiary cell.

the flow patterns and their effect on heat transfer. Lartigue et al. (2000) carried out experimental (PIV) and numerical studies (AR = 40, $3 \times 10^3 < Ra < 2 \times 10^5$) to focus on the evolution of circulation cells in the core of the cavity and showed that cells do not remain stationary but move downward. They attributed the movement of the cells due to the presence of rms (root mean square) fluctuating velocity in the horizontal direction (x-component). Further, they observed that the magnitude of the rms fluctuating velocity during secondary flow was 13% of the velocity of the primary flow and this caused a slow, ordered movement of the cells. Chan et al. (2004) presented a comprehensive description for the genesis of cells based on the change in the fluid kinetic energy. They conducted experiments in a tall tank of AR = 15 (interior dimensions 225 mm high × 15 mm wide × 75 mm deep) and validated their experimental results with numerical prediction by solving two-dimensional stream vorticity equations (Table 1C). They took 20 snapshots over a time period of 1200 s each at an interval of 60 s. They found that, the convection cells are generated periodically at the upper and lower portions of the tank and then migrate towards the center. The reason for this migration has been explained by Chan et al. (2004) in terms of the local pressure gradients.

1.2. Motivation

The literature survey has shown that a considerable amount of research has been carried out both numerically and experimentally with air-filled cavities and cavities filled with low and high Pr number fluids. Over the years, a considerably better understanding has been developed to explain the vertical temperature gradients inside the cavity, the flow of the core, the temperature and velocity distribution at the wall layers and the effect of endwalls and boundary conditions. Recently, researchers (Le Quéré, 1990; Wakitani, 1997; Chan et al., 2004) have concentrated their effort in understanding the unsteadiness of flow in the core region of the cavity. Some challenges like the role of the dimensionless numbers (Ra, Pr and AR) (the ratio of viscous to buoyancy forces; pressure forces and the ratio of the momentum to heat diffusivities) in the formation and disappearance of circulation cells, their unsteady behavior and transformation from unicellular to multicellular pattern still remain unsolved. Also, the theory behind the genesis of the cells given by Chan et al. (2004) (due to a small reduction in pressure force as compared to shear and buoyancy forces) was proposed for ethanol–water system and needs to be confirmed with fluids of different Pr number as working fluids.

The present work mainly focuses on the issues such as: (1) develop an energy balance for the present system (2) dependency of Gr_c on Pr number of fluids on flow patterns, (3) analysis of unsteady nature of cells, i.e., variation of number of cells with time and (4) role of pressure gradients in the cell formation over a wide range of Pr number of fluids. Most of the explanations about these issues have come from analytical works which were limited in capability due to the assumptions involved essentially for mathematical simplicity. So to avoid any such assumptions computational fluid dynamics (CFD) has been used as a tool. CFD simulations have been carried out for four different fluids namely, mercury ($Pr = 0.024$), air ($Pr = 0.73$), water ($Pr = 7$) and silicon oil ($Pr = 224$). Predictions of air have been compared with published experimental (photographic) and numerical results. A good agreement in terms of qualitative and quantitative terms motivated us to perform simulations for other fluids ($0.02 < Pr < 250$). A width of 0.02 m and AR = 20 has been considered for all simulations.

2. Mathematical formulation

In the present work, the left wall of the vertical slot is maintained at a constant temperature, (T_h) while the right wall is maintained at a constant temperature T_c, and ($T_h > T_c$). Following are the assumptions made in the present work.

1. Fluids are assumed to be incompressible and Newtonian.
2. The flow is assumed to be two-dimensional.
3. Properties of the fluid except viscosity do not change significantly in temperature range: $T_c < T_m < T_h$ where $T_m = 300$; $292 < T_c < 299$; $301 < T_h < 308$ (Table 2 A and B).
4. All the working fluids are operated at temperature differences within Boussinesq approximation. The well-known Boussinesq equation has been employed and the density in

Table 2
(A) Properties of working fluids; (B) temperatures applied at boundaries for different cases considered

Fluid	Density ρ (kg m^{-3})	Specific heat C_p (J kg^{-1} K^{-1})	Kinematic viscosity v (m^2 s^{-1})	Thermal diffusivity α(m^2 s^{-1})	Thermal expansion coefficient β (1/K)	Temperature T (K)
(A)						
Mercury	1.35E + 04	1.39E + 02	1.15E − 07	4.40E − 06	1.82E − 04	3.00E + 02
Air	1.23E + 00	1.01E + 03	1.54E − 05	2.48E − 05	3.45E − 03	3.00E + 02
Water	9.98E + 02	4.19E + 03	1.00E − 06	1.50E − 07	2.70E − 04	3.00E + 02
Silicon oil	8.72E + 02	1.72E + 03	2.00E − 05	8.95E − 08	1.12E − 03	3.00E + 02

(B)

Fluid	Temperatures (K)		
	T_c	T_m	T_h
Mercury	292	300	308
Air	292	300	308
Water	298.5	300	301.5
Silicon oil	292	300	308

Table 3
Values of constants used in the relation of viscosity varying with temperature

Fluid	Constants		
	A	B	C
Water	−10.2158	1.79E + 03	1.77E − 02
Silicon oil	143.2135	4.97E − 01	–

the buoyancy term is assumed to vary with the temperature according to the following relation:

$$\rho = \rho_0(1 - \beta(T - T_0)), \tag{1}$$

$$\beta = \left[\frac{1}{\rho}\left(\frac{\partial\rho}{\partial T}\right)\right]. \tag{2}$$

5. Heat transfer by radiation has not been included since the temperature difference considered is low for any significant radiation to occur.
6. Length of enclosure is sufficiently large for two-dimensional motion to be assumed.
7. Variation in viscosity is assumed as a function of temperature.

For water: $\mu = A + B/T + CT$, (3)

For silicon oil: $\mu = A - BT$, (4)

where A, B, C are constants and T is the temperature (Table 3).

2.1. Non-dimensional governing equations

The dimensionless length, AR, velocities, pressure, temperature and time are given by the expressions given below. Fig. 3 A shows the schematic of the grid of a rectangular slot considered in the present work while Fig. 3B shows the magnified view of

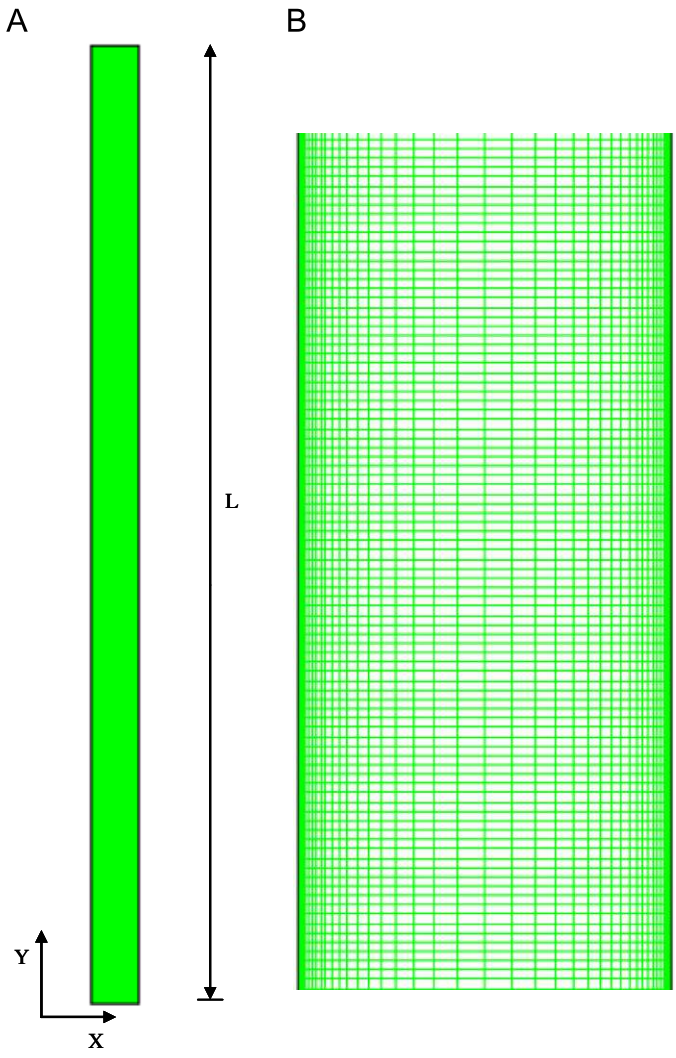

Fig. 3. Sample grid. (A) AR = 20; (B) magnified view.

Table 4
Boundary conditions and the model equations used for 2D model

2D	Equations	Boundary conditions
Mass balance	$\rho\left(\frac{\partial u}{\partial x}+\frac{\partial v}{\partial y}\right)=0$	Initial velocity condition: $u(x,y,0)=v(x,y,0)=0$ for $0\leqslant x\leqslant 0.02,\ 0\leqslant y\leqslant 0.4$ Initial temperature condition: $T(x,y,0)=0$ for $0\leqslant x\leqslant 0.02,\ 0\leqslant y\leqslant 0.4$ Initial x-direction boundary conditions: $u(x,0,t)=v(x,0,t)=0$ for $0\leqslant x\leqslant 0.02$ and $t\geqslant 0$
Momentum balance	In x-direction $\rho\left(\frac{\partial u}{\partial t}+u\frac{\partial u}{\partial x}+v\frac{\partial u}{\partial y}\right)$ $=-\frac{\partial p}{\partial x}+\left\{\frac{\partial}{\partial x}\left[\mu\frac{\partial u}{\partial x}\right]+\frac{\partial}{\partial y}\left[\mu\frac{\partial u}{\partial y}\right]\right\}$	Final x-direction boundary conditions: $u(x,0.4,t)=v(x,0.4,t)=0$ for $0\leqslant x\leqslant 0.02$ and $t\geqslant 0$ Final y-direction boundary conditions: $u(0,y,t)=v(0,y,t)=0$ for $0\leqslant y\leqslant 0.4$ and $t\geqslant 0$ Final y-direction boundary conditions: $u(0.02,y,t)=v(0.02,y,t)=0$ for $0\leqslant y\leqslant 0.4$ and $t\geqslant 0$ $300<T(0,y,t)<308$ for $0\leqslant y\leqslant 0.4$ and $t\geqslant 0$ $292<T(0.02,y,t)<300$ for $0\leqslant y\leqslant 0.4$ and $t\geqslant 0$ $\frac{\partial T(x,0,t)}{\partial y}=\frac{\partial T(x,0.4,t)}{\partial y}=0$ for $0\leqslant x\leqslant 0.02$ and $t\geqslant 0$
	In y-direction $\rho\left(\frac{\partial v}{\partial t}+u\frac{\partial v}{\partial x}+v\frac{\partial v}{\partial y}\right)$ $=-\frac{\partial p}{\partial y}+\left\{\frac{\partial}{\partial x}\left[\mu\frac{\partial v}{\partial x}\right]+\frac{\partial}{\partial y}\left[\mu\frac{\partial v}{\partial y}\right]\right\}+g\beta\Delta T$	
Energy balance	$\frac{\partial T}{\partial t}+u\frac{\partial T}{\partial x}+v\frac{\partial T}{\partial y}=\alpha\left(\frac{\partial^2 T}{\partial x^2}+\frac{\partial^2 T}{\partial y^2}\right)$	

non-uniform (larger number of grid cells near the wall) grid in the simulation.

$$X=\frac{x}{L},\quad Y=\frac{y}{L}, \tag{5}$$

$$U=\frac{u}{V_0},\quad V=\frac{v}{V_0}\quad \text{where } V_0=\sqrt{g\beta\Delta TL}, \tag{6}$$

$$P=\frac{p}{\rho V_0^2},\quad \theta=\frac{T-T_m}{T_h-T_c},\quad t^*=\frac{t}{t_0}\quad \text{with } t_0=\frac{L}{V_0}. \tag{7}$$

The transient governing equations (dimensional) are given comprehensively in Table 4.

2.2. Method of solution

The laminar model equations described above have been solved using commercial flow simulation software FLUENT (version 6.2) (FLUENT, 2005). Transient simulations have been carried out with a time step of 0.0001 s. For each time step, convergence criteria for sum of normalized residues have been set to 1×10^{-4} for continuity equations, 1×10^{-4} for momentum and 1×10^{-7} for energy equations. Convergence has been ensured at every step. The under-relaxation parameters were set to 0.3 for pressure, 1 each for density, energy and body forces and 0.7 for momentum equations. In this study a segregated solver with implicit time discretization has been employed for obtaining the solution of momentum equations. The momentum equations were discretized using the third-order MUSCL scheme and for pressure equation, PRESTO scheme was used. The third-order MUSCL scheme (Monotone Upstream Centered Schemes for Conservation Laws) which blends central differencing scheme and third-order upwinding scheme has been used since it gives faster convergence. It is given by the expression

$$\phi_f=\theta'\bar{\phi}_f+(1-\theta')\phi_{f,\mathrm{SOU}}, \tag{8}$$

where ϕ represents any scalar or vector quantity like temperature, pressure and velocity, and θ is the weighting factor.

This scheme prevents numerical diffusion while taking care of the fact that it does not dampen the disturbances which cause the instability. Thus, it ensures spatial accuracy.

To test the grid sensitivity, simulations were carried out for different grid sizes (not reported) with non-uniform grids, fine near the walls and relatively coarse in the middle. Since a constant vertical slot width of 0.02 m was selected for all the simulations the width has been divided into 40 parts with grids at the middle 5 times the grid near the wall. The sample grid for an AR = 20 is shown in Fig. 3B with a magnified view to show grid sizes. For example if the height was 0.4 m it was divided into 800 parts. Thus for AR = 20 a grid of 40×800 was used.

When heat is supplied gradually to a stagnant fluid the numerical run is said to be gradual. In a gradual run the data from the previous numerical run is considered as initial data and fed to the numerical run for a higher temperature difference. The importance of a gradual run was emphasized by Lee and Korpela (1983) who carried out simulations with water. It was noted that initial data provided a better understanding of the instability, induced later and agreed well with the experimental data available in literature.

When heat is supplied instantaneously to the stagnant fluid located in the slot from one side the Computational Fluid Dynamics (CFD) run is said to be impulsive. In such type of CFD runs each run is independent from the other runs (it does not

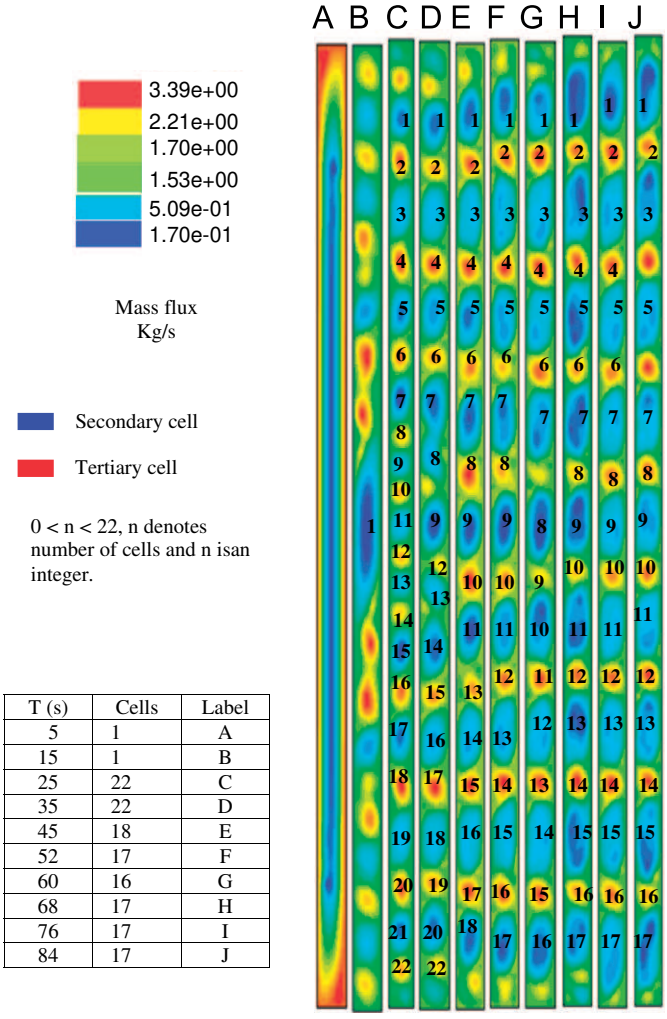

T (s)	Cells	Label
5	1	A
15	1	B
25	22	C
35	22	D
45	18	E
52	17	F
60	16	G
68	17	H
76	17	I
84	17	J

Fig. 4. Time sequence of the stream function field for mercury: Ra=397, 450; AR = 20. (A) $t = 5$ s; (B) $t = 15$ s; (C) $t = 25$ s; (D) $t = 35$ s; (E) $t = 45$ s; (F) $t = 52$ s; (G) $t = 60$ s; (H) $t = 68$ s; (I) $t = 76$ s; (J) $t = 84$ s.

depend on the initial data). Numerically, a temperature difference is applied at time $t = 0$ s and allowed to proceed till quasi-steady state in hydrodynamic condition is achieved. Wakitani (1996) measured the vertical velocity at a point near the wall for this purpose and monitored it for the entire time period of performing the experiment as well as for an impulsive run. The fluctuations of vertical velocity caused due to instability matched both experimentally and numerically. Thus an impulsive run is considered as a better measure for predicting flow patterns and was considered for the simulations.

3. Energy balance

Average rate of viscous energy dissipation by a unit section of fluid is given by

$$E_v = -\rho\nu \int_0^L [\langle u\nabla^2 u\rangle + \langle v\nabla^2 v\rangle]\,\mathrm{d}z. \tag{9}$$

Average rate of energy released by buoyancy per unit length of the fluid is given by

$$E_b = -\rho g\beta \int_0^L [\langle \Delta T v\rangle]\,\mathrm{d}z. \tag{10}$$

The average rate of energy released by pressure disturbances per unit length of the fluid is given by

$$E_p = -\int_0^L \left[\left\langle \frac{\Delta p}{\Delta x} v\right\rangle\right] \mathrm{d}z. \tag{11}$$

The balance theorem by Chandrashekhar (1961) says that "The instability occurs at the minimum temperature gradient at which balance can be steadily maintained between kinetic energy maintained by viscosity and internal energy released by the buoyancy force." Here the averages of the pressure distributions are considered to be zero. The balance theorem by Chandrashekhar (1961) can be written as

$$E_v = E_b. \tag{12}$$

In the present work it has been found that the pressure gradient term makes a significant contribution to the formation of cells and hence their averages cannot be considered as zero. The magnitude of the viscous and buoyancy forces is much higher than that of the pressure forces but for lateral flow there should be a lateral pressure gradient. The smallest change in the magnitude of two lateral points on pressure line will cause instability. Let us at this point assume an energy balance given by

$$E_v = E_b + E_p. \tag{13}$$

4. Results and discussions

Flow patterns at different times are obtained from numerical simulations and are shown in Section 4.1. The physics behind the formation of cells and the moving and merging of cells has been discussed. A criterion for the prediction of critical Gr_c on the basis of Pr number has been established.

4.1. Hydrodynamics

In this subsection results of hydrodynamics of the system have been summarized, and an attempt has been made to understand the corresponding physics of the phenomenon.

4.1.1. Formation, moving and merging of cells

The study of hydrodynamics of the system has been carried out in an ascending order of Pr number of the fluid. The numerical simulations presented in this section are performed for a constant AR (AR = 20).

Fig. 4 shows the stream function plots for mercury as a fluid in a vertical slot ($Ra = 3, 97, 450$). For low Pr number fluids ($0.001 < Pr < 0.1$) the critical Rayleigh number $Ra_c = 15,000$ (Lee and Korpela, 1983). Presently, Ra has been selected in super-critical range (above $10Ra_c$) to visualize the tertiary flows as visualized by Elder (1965). An unicellular

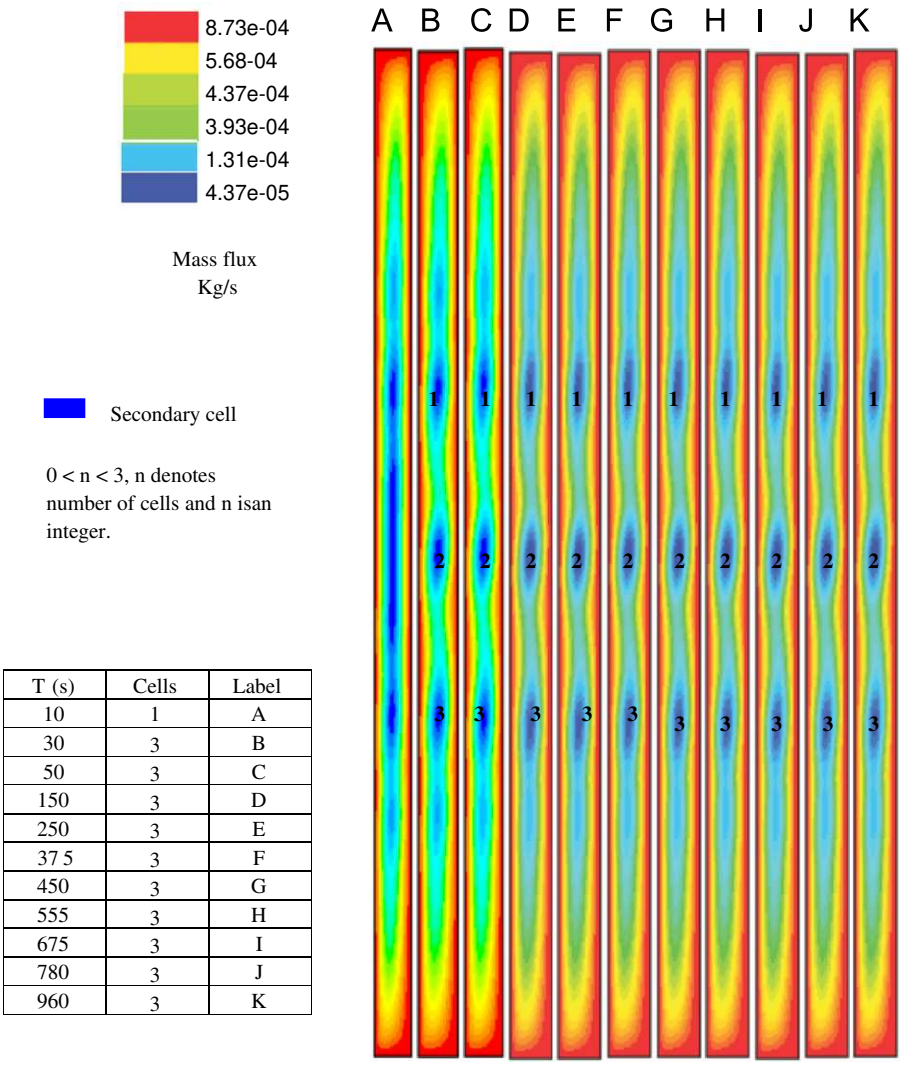

T (s)	Cells	Label
10	1	A
30	3	B
50	3	C
150	3	D
250	3	E
37 5	3	F
450	3	G
555	3	H
675	3	I
780	3	J
960	3	K

Fig. 5. Time sequence of the stream function field for air: $Ra = 11,735$; AR = 20. (A) $t = 10$ s; (B) $t = 30$ s; (C) $t = 50$ s; (D) $t = 150$ s; (E) $t = 250$ s; (F) $t = 375$ s; (G) $t = 450$ s; (H) $t = 555$ s; (I) $t = 675$ s; (J) $t = 780$ s; (K) $t = 960$ s.

pattern is observed just 5 s (Fig. 4A) after the temperature difference is applied in an impulsive run. Instability sets in rapidly at 10 s (Fig. 4B) and parallel convection rolls similar to Rayleigh–Benard cells (Koshmieder, 1993) are observed. The moving and merging of cells can be observed from the changing number of cells (Fig. 4). The cells are arranged in an adjacent cell pair (secondary–tertiary cell) rotating in opposite direction. The appearance and disappearance of tertiary cells and increase and decrease in size of the secondary cells can be seen (Fig. 4A–J). A quasi-periodic behavior is seen with the progress in time.

Fig. 5 shows the various flow patterns of air in a vertical slot of AR = 20 and $Ra = 1.1735 \times 10^4$. A unicellular pattern is seen up to $t = 10$ s (Fig. 5A). The onset of instability takes place after 15 s. At the end of 30 s (Fig. 5B) three cells are seen. The same number of cells is seen for a period of about 960 s (Fig. 5K) with no further change in its size or number. A considerable work on air as a fluid can be found in the literature (Le Quéré, 1990; Wakitani, 1994, 1996; Zhao et al., 1997; Lartigue et al., 2000). The present flow patterns agree with those of Le Quéré (1990), who showed three cell patterns for $Ra = 2 \times 10^4$ and AR = 16. The operating regime has been chosen to be in the multicellular regime as suggested for the conditions considered by Zhao et al. (1997). At low AR ($AR \leqslant 20$) and low Rayleigh number ($Ra \leqslant 20,000$) the fluids have been found to be sensitive to initial conditions and conditions when an impulsive temperature difference is applied.

Fig. 6 shows the multicellular regime for air as given by Zhao et al. (1997). The present work has been carried out within the multicellular regime.

Fig. 7 shows the various flow patterns for water in a vertical slot of AR = 20 and $Ra = 4.45 \times 10^5$. The solution scheme used in the present work was first checked for the simulations of Lee and Korpela (1983) ($L = 0.015$ m, AR = 20 and $Gr = 40,000$). The simulations carried out in the present work are for a slightly higher Ra, slightly higher width ($L = 0.02$ m) and lower AR. The figure further depicts that as the time increases the cells keep on forming and merging. At $t = 60$ s

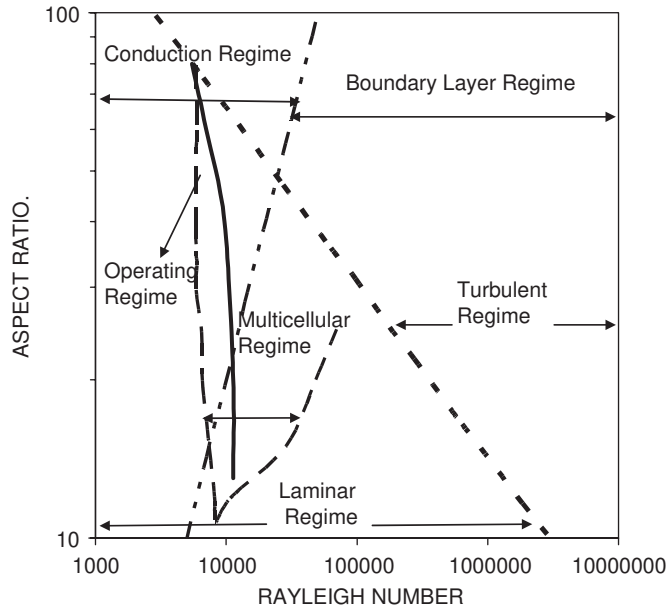

Fig. 6. Various regimes of operation of air and the current operating regime. Batchelor (1954) ▬ · ■ ■; Yin et al. (1978) ▬ ▬; Zhao et al. (1997) ▬ ▬; Present work ▬.

(Fig. 7A) four cells have been observed where as at $t = 147$ s (Fig. 7M) six cells have been observed. The cell merging and breaking process continues and at $t = 325$ s (Fig. 7U) the number of cells seen is eight. Simulations after $t = 280$ s have also been carried out and the same quasi-periodic behavior has been noted.

Fig. 8 shows the transient simulation for high Pr number fluids such as silicon oil ($Pr = 224$, $Ra = 8.22721 \times 10^5$). It has been observed that the cell formation starts after a considerable elapse of time as compared to the fluids which have low viscosity. A single cell is seen at $t = 300$ s (Fig. 8A) after which the number of cells starts increasing and three distinct cells are seen at $t = 530$ s (Fig. 8E). A maximum of five cells are seen after $t = 725$ s (Fig. 8G). The cells then merge and form a single cell at $t = 1080$ s (Fig. 8M) and again a quasi-periodic behavior is seen.

4.1.1.1. Significance of pressure gradient in cell formation moving and merging of cells Figs. 9 (A)–(D) show the vertical distribution of pressure at different timescales. The role of pressure gradient can be explained as follows. Consider a tall vertical slot (AR = 20) in a state of rest at time $t = 0$. Within the slot the pressure is minimum at the center and maximum at either end. Assume a certain temperature gradient applied to the two side walls such that one side is heated and the other cooled symmetrically. As time proceeds the pressure values at the top and the bottom increase. However, magnitude of the pressure gradient is negligible, due to which instability does not occur and a unicellular flow structure is formed (Figs. 4A, 5A, 8A). In unicellular flow pattern, there is a good balance between the viscous and buoyancy forces and the flow can be considered as fully developed. As we increase the temperature gradient, the magnitudes of pressure forces increase and cause imbalance between the buoyancy and viscous forces. The small disturbances present in the slot are amplified by the pressure gradient to develop into convection cells. Once fully developed, the convection cells are maintained by buoyancy, since shear is completely dissipative. The lateral movement of the fluid across the slot takes place and multiple cells are formed with the passage of time. The flow then becomes fully developed and steady, retaining the multiple cells (Fig. 5B– K). As we further increase the temperature gradient the unicellular pattern is formed initially and then multiple cells are formed (7A–U). Pressure gradient also exists in the axial direction with lowest pressure at the center. Hence the cells at the two ends migrate due to the pressure gradient toward the center causing the merging of cells (height wrt Y axis) (e.g. Figs. 7F, G, M–P, 8G–K). When temperature gradient is further increased, tertiary cells are seen (Fig. 4C–J). With each cell merging the region of strong shear between the two merging cells vanishes, thereby reducing the shear dissipation in the slot.

Figs. 9A depicts that the pressure disturbances in the case of mercury as a fluid. The magnitude of these pressure disturbances increases or decreases according to the increase or decrease in size of the secondary and tertiary cells. The direction of the pressure is opposite for each adjacent cell pair (secondary and tertiary cell) which suggests that there exists a different mechanism for the generation of tertiary cells, which needs further investigation.

Figs. 9B and C show that the general shape of the curve of vertical pressure gradient remains the same with small variations at different times owing to the presence of convection cells. Thus, the pressure gradient within the slot is the cause of both cell genesis and cell merging process and the pressure work provides the energy needed for these two processes. In the top and bottom portions the rate of change of pressure energy is zero. The circulation in each convection cell will present local maxima of pressure in the mid-section owing to the convection cells. The imbalance is due to the increase in the pressure force and an increase in the kinetic energy. But Fig. 9D does not show the same pressure profiles as in Figs. 9B and C although the cell merging and moving process still persists. The pressure fluctuations are dampened due to high viscosity of silicon oil and hence are not visible. This suggests the existence of a relationship between the critical Gr number and Pr number in the range $0.71 < Pr < 7$ above which, tertiary flows can be seen. For $Pr > 50$ the relationship between critical Gr number and Pr number has been analyzed by Chan et al. (2004) with experimental data from the literature with AR = 15. It is observed that for AR = 20 there is a slight increase in the critical Gr ($Gr \approx 2Gr_c$).

4.1.1.2. Effect of prandtl number on cell moving and merging The Gr number above which the instability starts is the critical Gr number (Gr_c). As per the discussion in Section 4.1.1.1 cells are formed due to the imbalance between the viscous and buoyancy forces. As the temperature difference is increased the cells start moving and merging. This depends on Pr number of the fluid since the cell merging and moving takes place at high temperature differences ($\Delta T = 16\,^\circ$C) while for water for

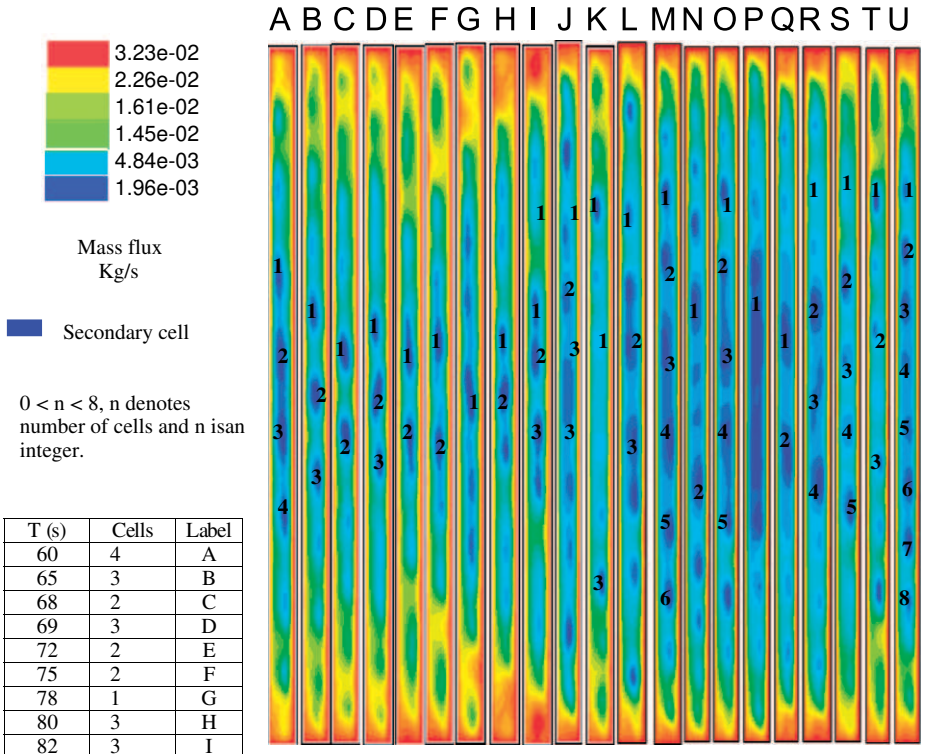

T (s)	Cells	Label
60	4	A
65	3	B
68	2	C
69	3	D
72	2	E
75	2	F
78	1	G
80	3	H
82	3	I
96	2	J
104	1	K
121	3	L
147	6	M
149	3	N
155	5	O
183	1	P
243	6	Q
244	4	R
250	3	S
255	5	T
325	8	U

Fig. 7. Time sequence of the stream function field for water ($Ra = 444,982$; AR = 20). (A) $t = 60$ s; (B) $t = 65$ s; (C) $t = 68$ s; (D) $t = 69$ s; (E) $t = 72$ s; (F) $t = 75$ s; (G) $t = 78$ s; (H) $t = 80$ s; (I) $t = 82$ s; (J) $t = 96$ s; (K) $t = 104$ s; (L) $t = 121$ s; (M) $t = 147$ s; (N) $t = 149$ s; (O) $t = 155$ s; (P) $t = 183$ s; (Q) $t = 243$ s; (R) $t = 244$ s; (S) $t = 250$ s; (T) $t = 255$ s; (U) $t = 325$ s.

example it takes place at relatively low temperature differences ($\Delta T = 3\,^{\circ}\mathrm{C}$). The moving and merging does not stabilize and continues in a quasi-periodic manner upto a Gr number specified as Gr_{cu}. There definitely has to be a criterion between these Gr numbers and Pr number. To understand this, simulations were carried out for Pr number in the range $0.71 < Pr < 7$ and critical Gr numbers at which the cell merging and moving took place were analyzed. For the above range of Pr and Gr numbers a power law relationship for the estimation of (Gr_{cu}) above which the cells are formed has been found and continue to move and merge has been obtained and is given by

$$Gr_{cu} = 23307 Pr^{1.36}, \quad 0.71 < Pr < 7. \tag{14}$$

It may be noted that the critical Gr number (presently represented as Gr_{cu}) above which unsteadiness has been described is reported as supercritical Gr number. For the convenience of determining the criterion of the contribution of pressure work we have used the notation Gr_{cu} which is above Gr_c. Thus we conclude that Eq. (13) is satisfied when $Gr \geqslant Gr_{cu}$ while Eq. (12) is satisfied for $Gr \geqslant Gr_c$.

Fig. 9D shows that the vertical distribution of dimensionless pressure against dimensionless vertical distance, the disturbances for a high Pr number fluid was not conspicuous since their magnitudes are very low. This prompted us to arrive at a conclusion that the viscous forces minimize the effect of the pressure forces for high Pr number fluids. Hence for $Pr > 50$ the relationship given by Chan et al. (2004) has been used to estimate the critical Grashoff number (Gr_c)

$$Gr_c = 2 \times 10^6 Pr^{-1.294}, \quad Pr > 50. \tag{15}$$

Chan et al. (2004) carried out simulations with ethanol–water solution ($Pr = 26$) and found that pressure differences play a major role in causing cell formation, moving and merging. From the present investigation it is difficult to estimate whether for a higher viscosity fluid like silicon oil ($Pr = 224$) the cell formation, moving and merging is depicted is due to pressure

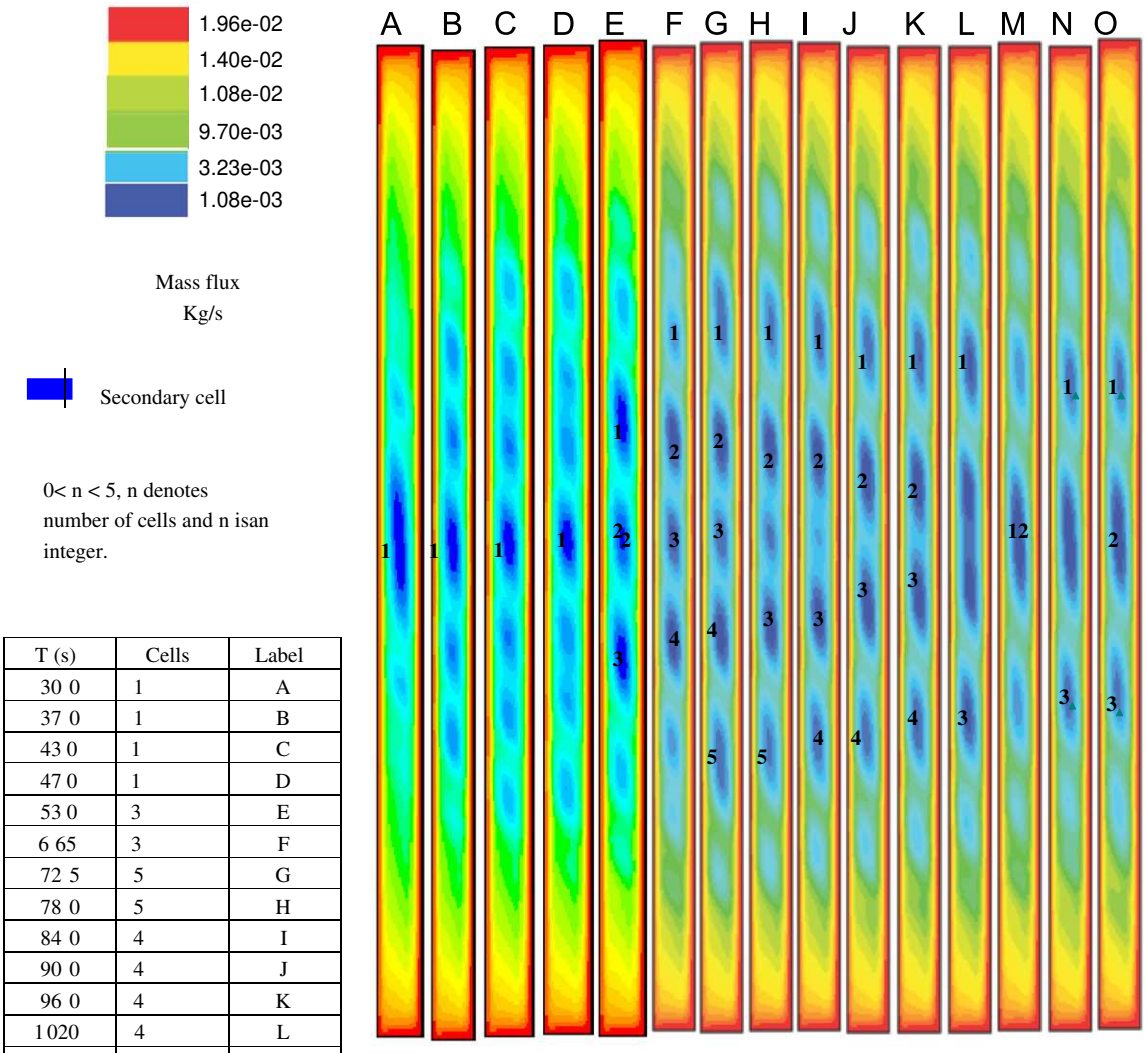

T (s)	Cells	Label
30 0	1	A
37 0	1	B
43 0	1	C
47 0	1	D
53 0	3	E
6 65	3	F
72 5	5	G
78 0	5	H
84 0	4	I
90 0	4	J
96 0	4	K
1 020	4	L
1 080	1	M
1 140	3	N
1 180	3	K

Fig. 8. Time sequence of the stream function field for silicon oil ($Ra = 822,721$; AR = 20). (A) $t = 300$ s; (B) $t = 370$ s; (C) $t = 430$ s; (D) $t = 470$ s; (E) $t = 530$ s; (F) $t = 665$ s; (G) $t = 725$ s; (H) $t = 780$ s; (I) $t = 840$ s; (J) $t = 900$ s; (K) $t = 960$ s; (L) $t = 1020$ s; (M) $t = 1080$ s; (N) $t = 1140$ s; (O) $t = 1180$ s.

work. Efforts are on to investigate the significance of pressure work in the case of high prandtl number fluids.

4.1.1.3. Effect of viscosity variation Figs. 10 and 11 show the plot of dimensionless y-velocity (vertical component of velocity) verses dimensionless time. The variation of viscosity with temperature gives variation at smaller timescales ($t^* < 250$) compared to the assumption of constant viscosity. For constant viscosity the variations are seen at much higher timescales ($t^* > 250$) which are not evident in the figure. A similar analysis was made by Wakitani (1996) who investigated the effect of viscosity variation with temperature of air at high Ra number ($Ra = 1 \times 10^6$). The viscosity of air increases with temperature whereas it decreases with temperature for silicon oil. Although for the temperature difference considered here, the effect of viscosity is very low, the lowering of viscosity due to temperature gradient in silicon oil is pronounced than that in air. To confirm this viscosity variation in silicon oil has been studied by monitoring the vertical velocity at a point ($x = 0.5$ mm, $y = 200$ mm) near the boundary layer. The vertical velocity for both the constant viscosity and variable viscosity case was monitored. It was found that there is very minute variation ($< 2\%$) in the linear velocity due to the variation in viscosity. For the rest of the fluids the variation in viscosity with temperature is found to be insignificant since with the assumption of constant viscosity the simulation results are almost identical.

4.1.2. Unsteady nature of cells

As seen from the analysis of Section 4.1.1, cells formed show a quasi-periodic behavior. The quasi-periodicity was numerically analyzed with increasing Rayleigh number by Le Quéré (1990) and experimentally by Wakitani (1994, 1996). The bifurcation phenomenon was analyzed with an increase in Ra number.

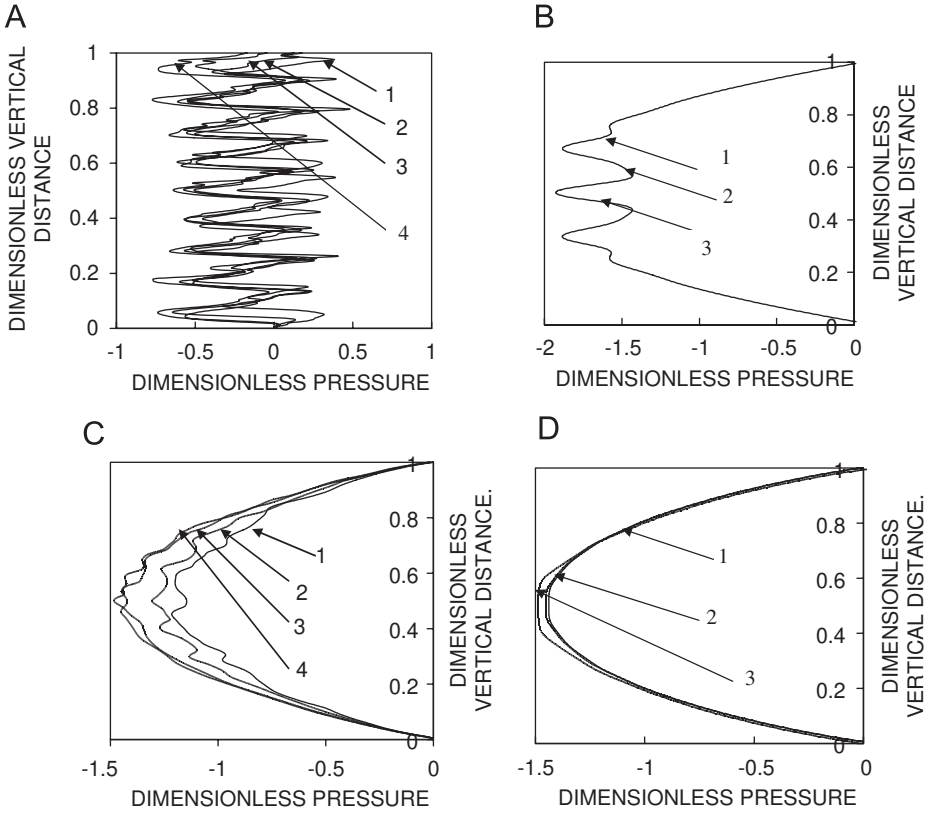

Fig. 9. Variation of pressure at the center of the cavity. (A) Mercury: 1. $t = 25$ s —; 2. $t = 60$ s –; 3. $t = 84$ s –; 4. $t = 106$ s –. (B) Air: 1. $t = 10$ s ——; 2. $t = 30$ s —; $t = 50$ s —. (C) Water: 1. $t = 60$ s ——; 2. $t = 80$ s –; 3. $t = 130$ s –; 4. $t = 140$ s ——. (D) Silicon oil 1. $t = 370$ s ——; 2. $t = 430$ s ——; 3. $t = 1080$ s ——.

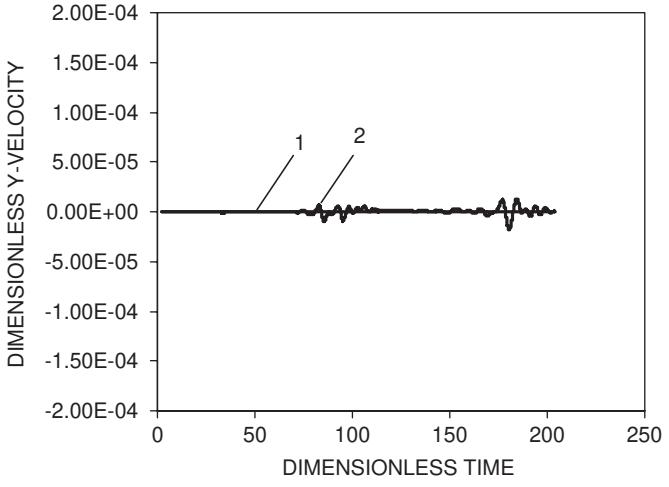

Fig. 10. Variation of viscosity for water. 1. —— Constant viscosity. 2. —— Variable viscosity.

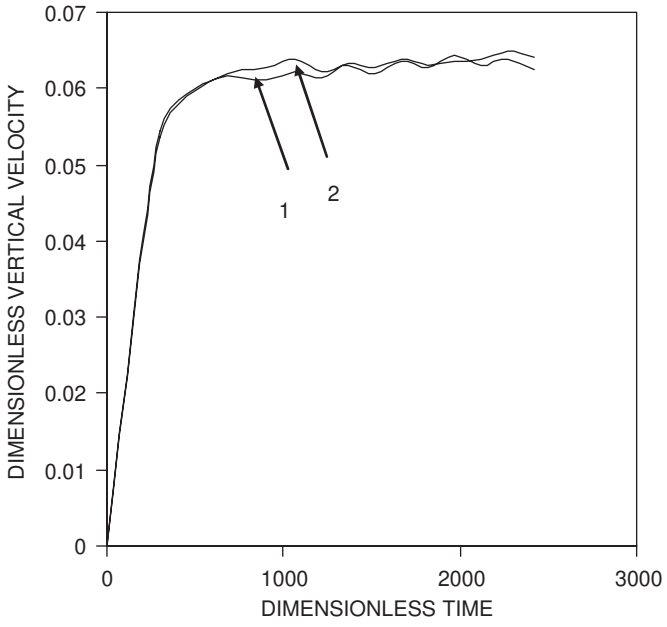

Fig. 11. Variation of viscosity for silicon oil. 1. —— Constant viscosity. 2. —— Variable viscosity.

Fig. 12A shows the quasi-periodic behavior of cells in the case of mercury as a fluid. Only secondary cells are considered with variation in time. Fig. 12B shows the behavior of cells in the case of air as a fluid and shows a steady behavior. Fig. 12C shows the unsteady behavior of cells for water as a fluid. At $Ra = 4.45 \times 10^5$, secondary cells repeat their merging and reappearance and their number changes from five to six or four to six (five–six cell mode). When Ra number is further increased, i.e., $Ra = 7.41636 \times 10^5$ two–three cell mode prevails. By this time tertiary cells appear but they are very weak to consider them as tertiary cells. At $Ra = 1.779926 \times 10^6$ transition

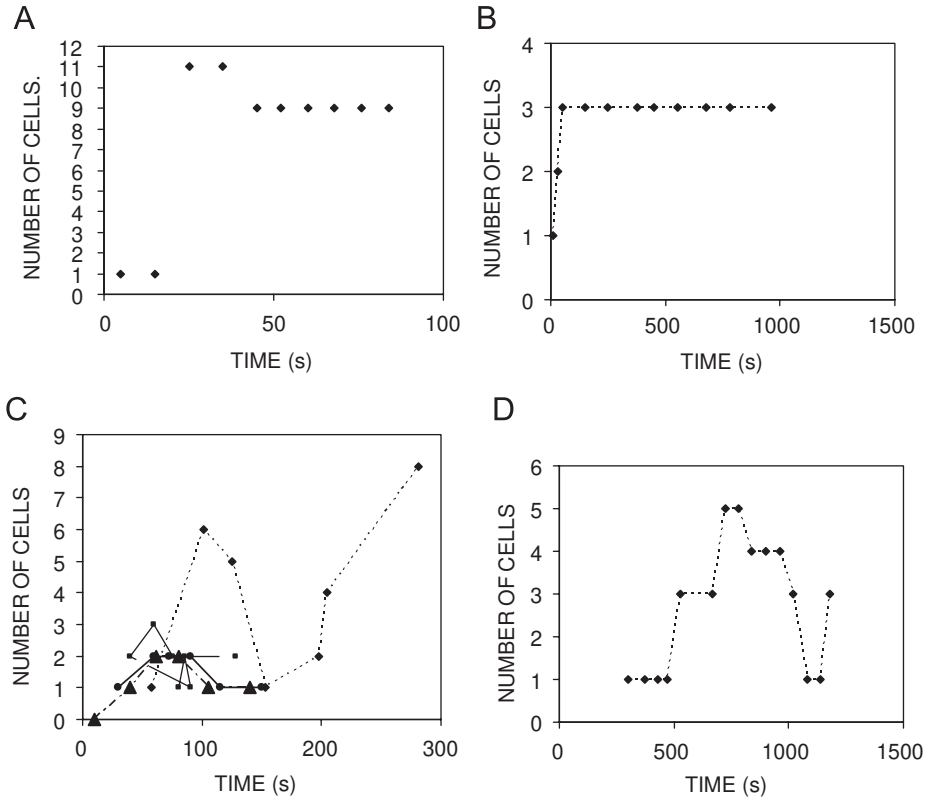

Fig. 12. Transient variation of number of cells with time. (A) Mercury: $Ra = 397,450$ --♦--. (B) Air: $Ra = 11,735$ --♦--. (C) Water: $Ra = 444,982$ --♦--; $Ra = 741,636$ —■—; $Ra = 1,779,926$ — ▲—; $Ra = 1,186,618$ — • —. (D) Silicon oil $Ra = 822,721$ --♦--.

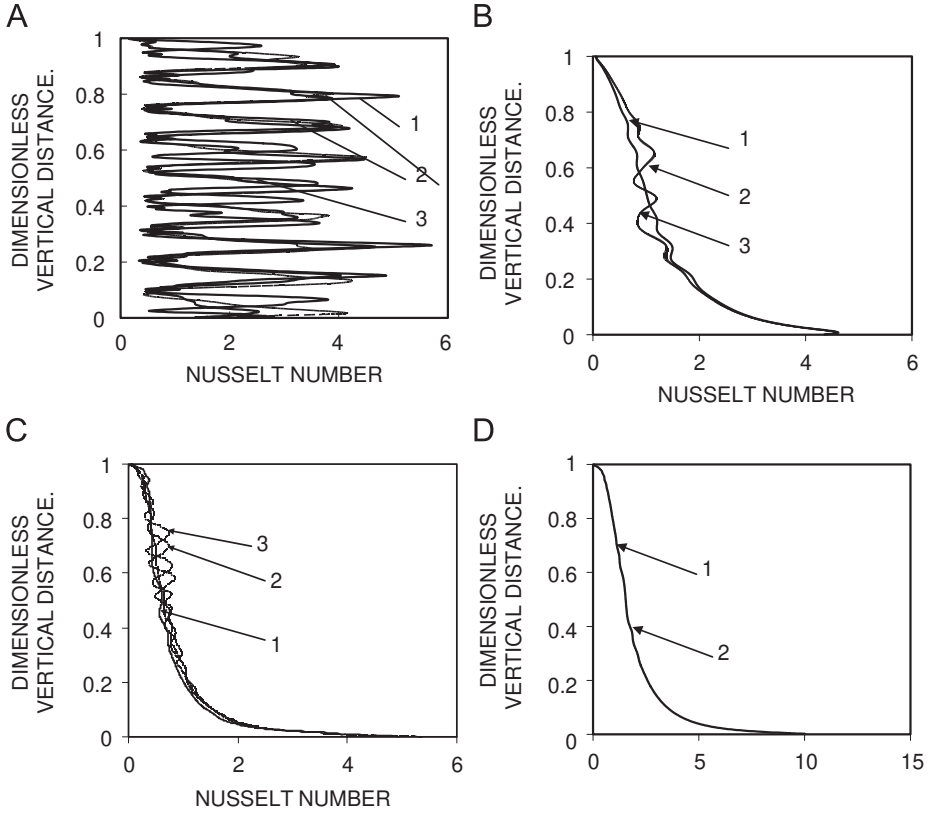

Fig. 13. Variation of Nusselt number (Nu) at the heated wall. (A) Mercury: 1. $t = 25$ s ———; 2. $t = 84$ s ———; 3. $t = 106$ s ———. (B) Air: 1. $t = 10$ s ———; 2. $t = 30$ s ———; 3. $t = 50$ s ———. (C) Water: 1. $t = 58$ s ———; 2. $t = 145$ s ———; 3. $t = 175$ s ———; 4. $t = 180$ s ———. (D) Silicon oil 1. $t = 370$ s ———; 2. $t = 430$ s ———.

from two to one cell takes place and two–one mode prevails. As the Ra number was further increased ($Ra = 4.45000 \times 10^5$ to $Ra = 3 \times 10^6$) it has been observed that the number of cells decreased. A similar trend of initial increase of cell number and then followed by a decrease with time was reported (Lee and Korpela, 1983). This is because due to the motion of the fluid the dynamic pressure decreases from the two ends to reach a minimum at the center of the slot. Lee and Korpela (1983) reported that with water as a working fluid, for $Ra = 2.80000 \times 10^5$, a pressure wave is generated, which carries away all the kinetic energy of the fluid and the cells break up resulting into an increase in number. As the time increases, the waves die out due to the viscous dissipation, the flow becomes fully developed and steady unicellular flow is maintained. Fig. 12D shows the smooth transition in the number of cells from six to one and then again six till 1200 s interval thus proving quasi-periodicity of cell formation and merging phenomena.

4.2. Heat transfer

Figs. 13B, C, and D show the Nu number variation at the hot wall with air, water and silicon oil, respectively as working fluids at different times. The data were taken at the time when cells are formed so that the enhancement in the Nu number due to the formation of cells may be understood. The fluctuations increase with time and are a function of the number of cells formed. The variation in Nu number shows an almost linear increase from top to bottom at timescales where cells have been formed as these fluctuations are consistent with number of cells.

The heat transfer in a vertical slot is calculated using Newton's law of cooling

$$h(T_h - T_c) = k_f \left(\frac{\mathrm{d}T}{\mathrm{d}x}\right). \tag{16}$$

The increase in the heat transfer coefficient is as follows: the hot fluid (lighter fluid) from the hot wall moves up and the cold fluid (denser fluid) near the cold wall moves down. In the hot zone at the top of the slot the temperature gradient is low and hence the heat transfer coefficient is low. In the bottom zone where the temperature is low due to the onward motion of the cold fluid the heat transfer coefficient is high. Hence we find the asymmetric nature of the Nu number at the hot wall in the case of all the fluids.

5. Conclusions

The present work has successfully captured the onset of multicellular patterns, instability mechanism in a vertical slot with fluids of different Pr number. For air and silicon oil the predictions of cellular patterns have been found to be in good agreement with the experimental data reported in the literature. The primary reason for the formation of cells during transition from laminar to turbulent at high Ra_c is addressed for fluids of different Pr number. The formation of tertiary cells is captured very well by CFD; but more insight into these require further investigation. The important observations from the present work are

1. Energy balance relating the viscous, buoyancy and pressure forces has been established.
2. Pressure disturbances play a significant role in the formation and merging of cells.
3. The unsteady nature of cells has been analyzed and a quasi-periodic behavior is seen.
4. The understanding for the cell formation and moving in the case of low Prandtl number like mercury and high Prandtl numbers like silicon oil needs further investigation.
5. A power law relation of Gr number with Pr number is established for the range $0.71 < Pr < 7$ and given by the following equation:

$$Gr_{cu} = 23307 Pr^{1.36}.$$

Notation

AR	aspect ratio (H/L)
C_p	specific heat of the fluid, J kg^{-1} K^{-1}
E	Energy, J m^{-1}
g	acceleration due to gravity, m s^{-2}
Gr	Grashoff number $\left(\frac{g\beta\Delta T \rho^2 L^3}{\mu^2}\right)$
h	convective heat transfer coefficient, W m^{-2} K^{-1}
H	height of the enclosure, m
i	direction co-ordinate
j	direction co-ordinate
k	thermal conductivity, W m^{-1} K^{-1}
L	width of enclosure, m
Nu	Nusselt number (hL/k)
p	pressure per unit surface, N m^{-2}
P	dimensionless pressure ($p/\rho V_0^2$)
Pr	Prandtl number $\left(\frac{C_p \mu}{k}\right)$
Ra	Rayleigh number ($g\beta\Delta TL^3/\nu\alpha$)
t	time, s
t_0	initial time, s, $t_0 = L/V_0$
t^*	dimensionless time, $t^* = t/t_0$
T	temperature, K
u	horizontal velocity, m s^{-1}
U	dimensionless horizontal velocity, u/V_0
v	vertical velocity, m s^{-1}
V	dimensionless vertical velocity, v/V_0
V_0	initial velocity, m s^{-1} ($V_0 = \sqrt{g\beta\Delta TL}$)
x	co-ordinate in x-direction, m
X	dimensionless horizontal length, x/L
y	co-ordinate in y-direction, m
Y	dimensionless vertical length, y/L

Greek letters

α	thermal diffusivity, m^2 s^{-1}
β	coefficient of thermal expansion, K^{-1}
δ	thermal boundary layer thickness

θ	dimensionless temperature, $\theta = T - T_m / T_h - T_c$
θ'	weighting factor
μ	dynamic viscosity, $\mathrm{kg\,m^{-1}\,s^{-1}}$
v	kinematic viscosity, $\mathrm{m^2\,s^{-1}}$
ρ	density, $\mathrm{kg\,m^{-3}}$
ϕ	any scalar or vector quantity

Subscripts

b	buoyancy
c	critical
cold	coldwall
cu	critical Grashoff number above which cells are formed
f	face cell
h	hot wall
m	mean
p	pressure
SOU	second order upwind
T	thermal
v	viscous

References

Batchelor, G.K., 1954. Heat transfer by free convection across a closed cavity between vertical boundaries at different temperatures. Quarterly of Applied Mathematics 12, 209–233.

Bergholz, R.F., 1978. Instability of steady natural convection in a vertical fluid layer. Journal of Fluid Mechanics 84 (4), 743–768.

Catton, I., 1978. Natural convection in enclosures. Proceeding of the Sixth International Heat Transfer Conference, vol. 6. pp. 13–31.

Chan, C.L., Yu, Y., Chen, C.F., 2004. Instability of convection of an ethanol–water solution in a vertical tank. Journal of Fluid Mechanics 510, 243–265.

Chandrashekhar, S., 1961. Hydrodynamic and Hydromagnetic Stability. Clarendon Press, Oxford.

Elder, J.W., 1965. Laminar free convection in a vertical slot. Journal of Fluid Mechanics 23, 77–98.

Elsherbiny, S.M., Raithby, G.D., Hollands, K.G.T., 1982. Heat transfer by natural convection across vertical and inclined air layers. Transactions of the ASME Journal of Heat Transfer 104, 96–102.

FLUENT 6.2., 2005. User's Manual to FLUENT 6.2. Fluent Inc. Centrera Resource Park, 10 Cavendish Court, Lebanon, USA.

Gill, A.E., 1966. The boundary layer regime for convection in a rectangular cavity. Journal of Fluid Mechanics 64, 515–536.

Korpela, S., Lee, Y., Drummond, J.E., 1982. Heat transfer through a double pane window. ASME Journal of Heat Transfer 104, 539–544.

Korpela, S.A., Gozum, D., Baxi, C.B., 1973. On the stability of conduction regime of natural convection in a vertical slot. International Journal of Heat and Mass Transfer 15, 1683–1690.

Koshmieder, E.L., 1993. Benard Cells and Taylor Vortices. Cambridge University Press, Cambridge, MA. pp. 11–35.

Lartigue, B., Lorente, S., Bourret, B., 2000. Multicellular natural convection in high aspect ratio cavity: experimental and numerical results. International Journal of Heat and Mass Transfer 43, 3157–3170.

Le Quéré, P., 1990. A note on multiple and unsteady solutions in two-dimensional convection in a tall cavity. Transactions of the ASME Journal of Heat Transfer 112, 965–973.

Lee, Y., Korpela, S., 1983. Multicellular natural convection in a vertical slot. Journal of Fluid Mechanics 126, 91–124.

Mull, W., Reiher, H., 1930. Der Warmeschutz von Luftschichten, Beihefte zum Gesundh.-Ing. Beihefte, Reihe 1, Heft 28.

Newell, M.E., Schmidt, F.W., 1970. Heat transfer by laminar natural convection within rectangular enclosures. Transactions of the ASME C: Journal of Heat Transfer 92, 159–167.

Quon, C., 1972. High Rayleigh number convection in an Enclosure—a numerical study. Physics of Fluids 15 (1), 12–19.

Rubel, A., Landis, F., 1969. Numerical study of natural convection in a vertical rectangular enclosure. Physics of Fluids Supplement II 12, 208.

Wakitani, S., 1994. Experiments on convective instability of large prandtl number fluids in a vertical slot. Journal of Fluid Mechanics 116, 120–126.

Wakitani, S., 1996. Formation of cells in natural convection in a vertical slot at large Prandtl number. Journal of Fluid Mechanics 314, 299–314.

Wakitani, S., 1997. Development of multicellular solutions in natural convection in an air-filled vertical cavity. Transactions of the ASME Journal of Heat Transfer 119, 97–101.

Yin, S.H., Wung, T.Y., Chen, K., 1978. Natural convection in an air layer enclosed within rectangular cavities. International Journal of Heat and Mass Transfer 21, 307–315.

Zhao, Y., Curcija, D., Gross, W.P., 1997. Prediction of multicellular flow regime of natural convection in fenestration glazing cavities. ASHRAE Transactions 103 (1), 1–12.